Proceedings of IGTI:
International Gas Turbine Institute
May 8-11, 2000 Munich, Germany

2000-GT-0121

AN EXAMINATION OF THE RELATIONSHIP BETWEEN CHEMILUMINESCENT LIGHT EMISSIONS AND HEAT RELEASE RATE UNDER NON-ADIABATIC CONDITIONS

Ludwig C. Haber, Uri Vandsburger, William R. Saunders, and Vivek K. Khanna

Reacting Flows Laboratory, Department of Mechanical Engineering,

Virginia Tech, Blacksburg VA 24060-0238

ABSTRACT

As combustion instability research has matured over the last decade the need for more detailed diagnostics has increased. One main gap in the diagnostics is the ability to obtain a reliable quantitative measure of unsteady heat release. In an effort to move in this direction using chemiluminescence as the measured quantity, this paper examines the formation of chemiluminescent light in the simple yet non-idealized environment of a Bunsen burner flame with co-flow of air. The results of the study show that OH* and CH* chemiluminescence can be modeled accurately using the simplified modeling approach outlined within the paper. The understanding of chemiluminescent light formation gained by the ability to model OH* and CH* light emissions accurately allows the correct interpretation of chemiluminescence in terms of heat release.

INTRODUCTION

To truly understand the nature of combustion instabilities the ability to measure the influence of acoustic velocity and pressure perturbations on flame heat release is indispensable. Chemiluminescence measurements have often been made to obtain some qualitative indication of the nature of the above described interaction (Samaniego et al., 1993). Quantitative heat release deductions from chemiluminescence measurements have also been made on a purely empirical basis, assuming a relationship between heat release and chemiluminescence without direct verification (Langhorne, 1987).

The formation and chemistry of chemiluminescent species has received some recent attention (Devriendt and Peeters, 1996) but is still not fully understood. In the case of OH*, the currently accepted mechanism was proposed by Broida et al. (1961) and has only been verified indirectly by Porter et al. (1962) and Dandy and Vosen (1992) among others.

Our study considers OH* and CH* as the main chemiluminescent species of interest. CO_2* has been studied as another possible indicator of heat release (Saminiego et al., 1995) but will not be discussed in this paper.

The present paper summarizes the first part of a study aimed at quantifying chemiluminescence measurements using a physically-based model capturing the major dependence of chemiluminescence on chemical kinetics and heat loss. Heat loss and mixture non-uniformity, specific to the experimental setup used in the study, are modeled empirically using parameterized, physically-based equations.

The experimental setup is briefly described in section one. Experimental results are given in section two. The chemiluminescence modeling approach is described in Section three. Section four presents the results of the modeling effort. Section five discusses the results obtained with respect to the use of chemiluminescence as a diagnostic tool. The discussion is summarized with conclusions concerning the use of OH* and CH* as heat release indicators in section six.

NOMENCLATURE

ϕ_{lean}	-	Lean equivalence ratio at flame edge
ϕ_{loc}	-	Local equivalence ratio at distance h
ϕ_{hom}	-	Equivalence ratio of incoming mixture
h	-	Distance along height of flame
θ	-	Measure of mixing layer thickness
q"	-	Heat loss per unit area
k	-	Conductivity of air
T_{flame}	-	Flame temperature
T_{rim}	-	Burner rim temperature
sd	-	Flame standoff distance
σ	-	Stefan-Boltzman constant (5.67×10^{-8})
ε	-	Nominal flame emissivity
T_{amb}	-	Temperature of surroundings

1. EXPERIMENTAL SETUP

The experimental setup chosen for this study is a laminar methane Bunsen flame with co-flow of air. The flame is stabilized on a 12 mm stainless steel tube, surrounded by a 100 mm diameter quartz tube that extends approximately 300 mm beyond the flame tip. The respective flows of air and methane are measured using mass-flow meters. The co-flow of air is controlled using a standard air rotameter.

Chemiluminescence is collected using a lens system coupled to a fiber optic cable. The lens system consists of two short focal length quartz lenses. The arrangement is optimized for even light transmission to the optical fiber from an area 5% larger than the exit area of the stainless steel tube. The arrangement assures, given the large ratio of object to lens distance to object depth that the same percentage of chemiluminescent light is captured from all of the flame. The fiber optic cable takes the collected light to a 0.5 m Ebert monochrometer. At the exit of the monochrometer a high sensitivity PMT converts the incident light flux to an electric current that is then amplified using an instrumentation amplifier and finally recorded by a PC based data acquisition system.

All light measurements presented in this paper have had a correction factor applied to them that accounts for the wavelength at which the measurement was made as well as for the fact that only a part of the total spectrum is measured at every point. The monochrometer acts as a narrow band-pass filter and therefore does not capture all radiation due to the chemiluminescent transitions. The proportion of the transitions captured at a given monochrometer wavelength setting within the transition range is a measurable function of the experimental conditions. Complete spectra were obtained to determine the function. The correction factor accounts also for the removal of background CO2* transition radiation from the desired OH* or CH* transition radiation.

The leanest mixture that can be stabilized in the above described configuration has an equivalence ratio of 0.7. The rich limit is not of interest in this study. The experimental study covers equivalence ratios in the range from 0.75 to 1.1 with air flow rates ranging from 55 to 70 cc/sec of air.

Two types of measurements were performed. One type of measurement is that of global chemiluminescence where a certain percentage of the light from all of the flame is captured, as introduced above. For the second type of measurement the area captured by the fiber optic was decreased to 2 mm^2, allowing measurements of the variation of chemiluminescence over the flame area. Both types of measurements are presented in this paper.

Since the measurements of chemiluminescence have been corrected for optical attenuation as well as for the variation of quantum efficiency of the PMT over changes in light wavelength, the values given for chemiluminescence are directly proportional to quantum yield from the flame. The remaining proportionality factor would account for a conversion of amplified voltage to PMT amperes, a conversion from amperes to incident light power assuming a 100% quantum efficiency and finally a factor relating the global chemiluminescence of the flame to the amount captured. All of these factors are constants within measurement uncertainty over all measurement conditions.

2. EXPERIMENTAL RESULTS

OH* and CH* global chemiluminescence results are shown as a function of equivalence ratio for several flow rates in Fig. 1 and Fig. 2 respectively. The co-flow of air was kept constant for all these measurements. The variation of chemiluminescence with equivalence ratio is very different for OH* and CH*, as can be expected from their production paths (discussed below). OH* peaks around stoichiometric burning conditions whereas

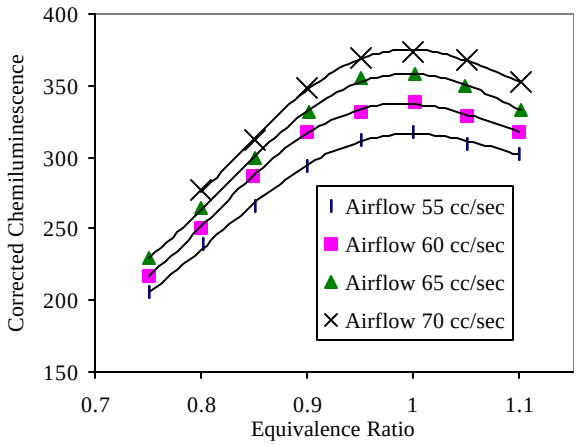

Figure 1. OH* chemiluminescence variation with equivalence ratio

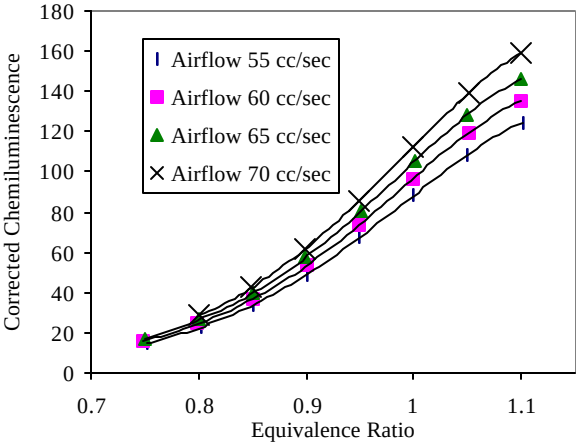

Figure 2. CH* chemiluminescence variation with equivalence ratio

CH* chemiluminescence has a maximum beyond an equivalence ratio of 1.1 on the rich side. Although not shown here, the variation of chemiluminescence with flow rate is linear. The slopes vary as a function of equivalence ratio for CH* and very weakly for OH*.

The need for local chemiluminescence measurements becomes apparent only after attempting to model the above experimental results. Nevertheless, local chemiluminescence measurements representing scans through the flame are presented at this point in order to obtain a complete experimental picture of the chemiluminescence characteristics of this type of Bunsen burner flame. The results were obtained by increasing the resolution of the experimental setup to $2mm^2$ and scanning diametrically through the flame.

Figure 3 shows the results for an OH* scan at an equivalence ratio of one with airflow of 60 cc/sec. The CH* scan for the same conditions is shown in Fig. 4. Both OH* and CH* vary widely over the radius of the burner. The variation

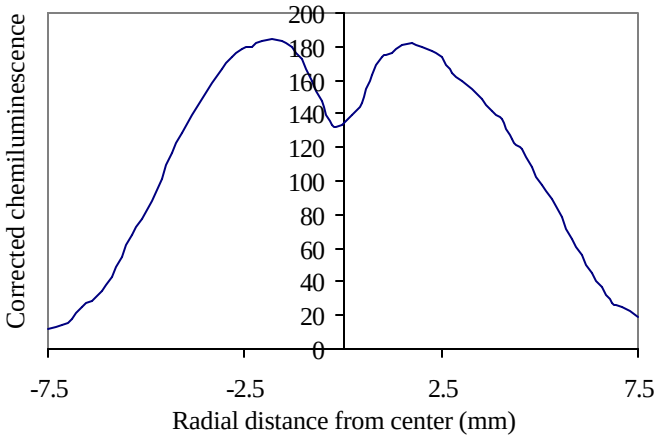

Figure 3. OH* chemiluminescence at $\phi = 1$ and an air flow of 60 cc/sec

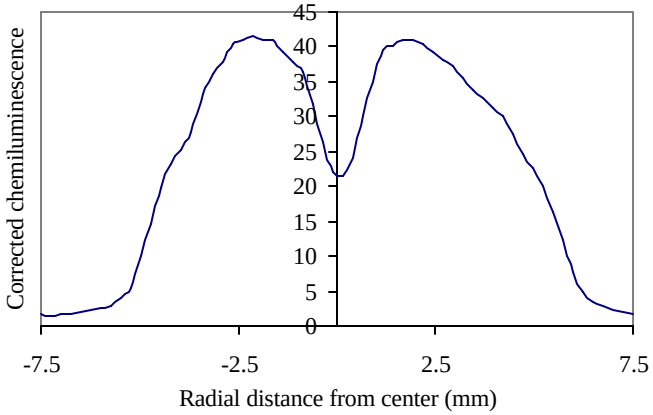

Figure 4. CH* chemiluminescence at $\phi = 1$ and an air flow of 60 cc/sec

affects the image collected for global chemiluminescence measurements. All of the radial non-uniformity is integrated into the measured value plotted in Fig. 1 and Fig. 2. Several factors influence the radial dependence of chemiluminescence. Leaning out of the flame due to mixing with the co-flow of air can be expected to affect the very outer edge of the flame. Heat loss to the burner rim plays a significant role in flame stabilization, especially for strong burning mixtures with relatively high flame speed (Sun et al., 1994). Flame curvature changes from convex to concave and affects the local heat loss from the flame and with it the chemiluminescence. Finally, the burning process near the flame tip appears very different from other parts of the flame given the local minimum in chemiluminescence for both OH* and CH*. All of these factors work together to give the chemiluminescence variation shown in Fig. 3 and Fig.4.

Without discussing these effects further it is clear that in order to model chemiluminescence the most dominant of the effects must be accounted for in some way. The ability to model the effects is crucial for the correct interpretation of chemiluminescence measurements.

3. CHEMILUMINESCENCE MODEL

To model chemiluminescence the main tool used is the Sandia 1-D flame code PREMIX (Kee et al., 1993) together with the improved methane combustion mechanism GRIMECH 3.0 (Smith et al., 1999). Nitrogen chemistry was not considered in the calculations. Added to the mechanism were the chemiluminescence production equations for CH* and OH* along with appropriate quenching and other consumption equations. The CH* production kinetics were taken from Devriendt and Peeters (1997). The quenching equations for CH* and OH* were guided by data in Garland and Crosley (1986).

The reaction for CH* formation is :

$$C_2H + O \Rightarrow CH^* + CO \qquad (1)$$

The reaction for OH* formation is:

$$HCO + O \Rightarrow OH^* + CO \qquad (2)$$

The OH* production equation used is not the commonly accepted reaction between CH and molecular oxygen. The detailed experimental evidence and reasoning in proposing reaction (2) as the production path are given elsewhere (Haber and Vandsburger, 2000).

In order to model the chemiluminescence observed in the experiments, several important assumptions are made. The most important assumption is that heat loss, although composed of radiative, conductive and convective components is dominated by conductive heat loss. It has been shown that radiative heat loss becomes important to flame structure only near flammability

limits which are not considered here (Egolfopoulos, 1994). Radiative heat loss is modeled as shown below but will be assumed to have the same effect on chemiluminescence as conductive heat loss. Convective heat loss is itself really a form of conduction and therefore will have a similar influence on chemiluminescence.

The second assumption is that the local behaviour of the flame can be modeled by a 1-D flame structure as calculated by PREMIX with local conductive heat loss and local mixture strength alone. Curvature of the Bunsen burner laminar flame only has significant effects near the flame tip. Curvature of the flame is therefore neglected in the present chemiluminescence model.

An important fact that contributes significantly to flame tip burning conditions is the preheating of the unburned mixture in the concave flame tip region. The preheating effect was neglected in the modeling study.

Finally, the last major assumption concerns the parameterization of the variation of local equivalence ratio over the flame area (accounting for leaning out at the flame edge) and the variation of local heat loss over the flame area.

Variation of equivalence ratio over the height of the flame was modeled as follows:

$$f_{local} = f_{lean} + \frac{f_{nom} - f_{lean}}{e^{a\,q}} \cdot \left(e^{a \cdot h} - 1\right) \qquad (h \le q)$$
$$f_{local} = f_{nom} \qquad (h > q) \qquad (3)$$

Three parameters govern Equation 3. α governs the slope of the variation of ϕ_{local} with flame height. The parameter was fixed at a value of 30. ϕ_{lean} represents the leanest burning at the edge of the flame; θ is a measure of the thickness of the co-flow mixing layer.

The variation of heat loss along the height of the flame is given by:

$$q'' = k \cdot \frac{T_{flame} - T_{rim}}{h + d_{sd}} + s \cdot e \cdot \left(T_{flame}^4 - T_{amb}^4\right) \qquad (4)$$

Two parameters govern Equation 4. T_{rim} represents the influence of the burner rim temperature. d_{sd} models the influence of flame standoff distance on heat loss. T_{amb} is the ambient temperature and is set equal to 298 ^{o}K. T_{flame} is not a parameter and is iteratively determined together with heat loss itself. The relationship between T_{flame} and heat loss is given by the PREMIX modeling results. The emissivity of the flame was considered constant at 0.005.

All of the parameters may vary with flow rate and equivalence ratio. Although the number of parameters thus exceeds the number of data points, the physical significance of the parameters restricts the choice of each in every case. The results shown below further illustrate this matter.

To obtain a database for how chemiluminescence varies with equivalence ratio for a range of heat loss magnitudes, a series of burner stabilized flame calculations were performed. Using the database and 2-D interpolation, a variation of heat loss and equivalence ratio along the flame height can be prescribed and integrated. The local speed of propagation of the flame was taken to be equal to the flame velocity under the modeled 1-D heat loss conditions. The flame height was calculated by matching the total integrated fuel consumption of the flame to the various test conditions. Once the flame height is determined total, global OH* and CH* chemiluminescence can be calculated by integration.

4. CHEMILUMINESCENCE MODELING RESULTS

The final calibration factor mentioned above, needed to convert the corrected chemiluminescence measurement to the quantum yield that is the output of the model, was fixed at an equivalence ratio of 1 and flow rate of air of 60 cc/sec. Any further variation of chemiluminescence was calculated using the model parameters discussed above. In order to make model comparisons meaningful, not only the model comparison to data will be shown but also the variation of parameters used to obtain these modeling results.

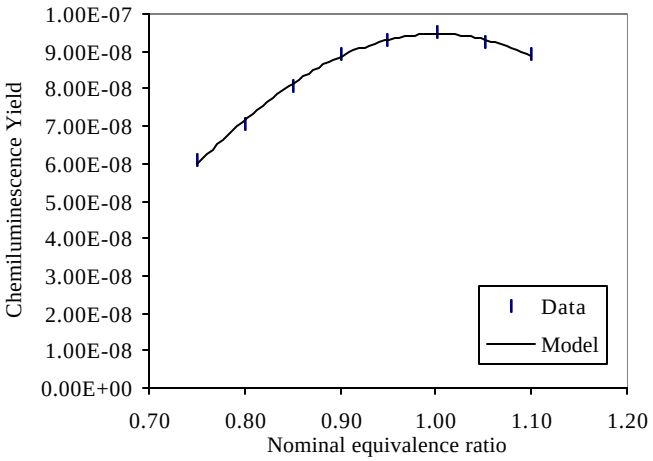

Figure 5. Comparison of modeled and experimental OH* chemiluminescence variation with nominal equivalence ratio

Modeling results at the experimental flow rate of 60 cc/sec of air are shown for OH* and CH* in Fig. 5 and Fig. 6 respectively. The OH* modeling effort was very successful whereas the CH* chemiluminescence model shows some discrepancy in following the data dependence on equivalence ratio.

Figures 7 and 8 show how the model predicts chemiluminescence variation with air flow rate for OH* and CH*

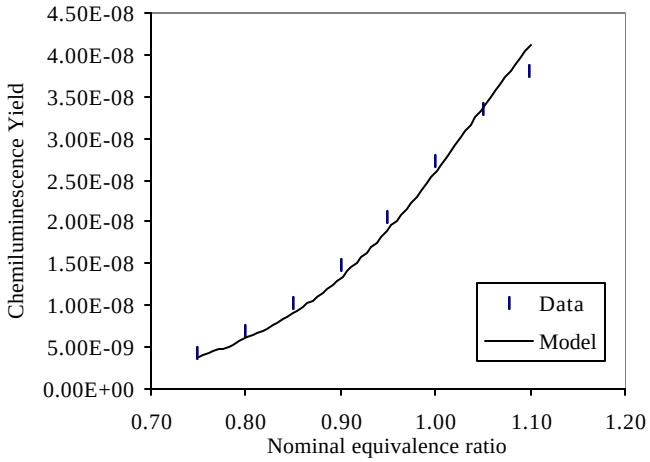

Figure 6. Comparison of modeled and experimental CH* chemiluminescence variation with nominal equivalence ratio

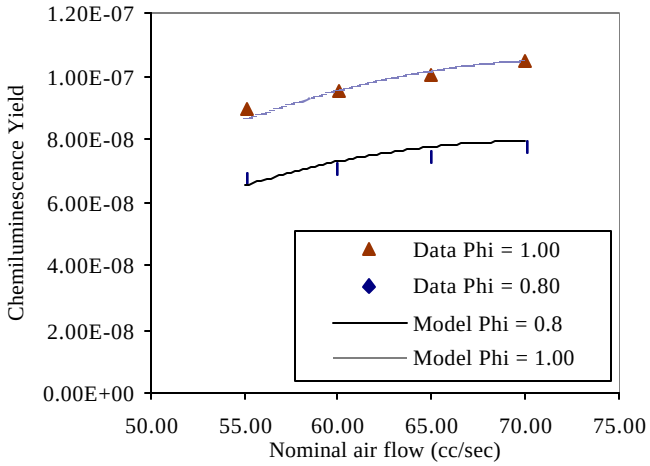

Figure 7. Comparison between modeled and experimental OH* chemiluminescence variation with nominal air flow

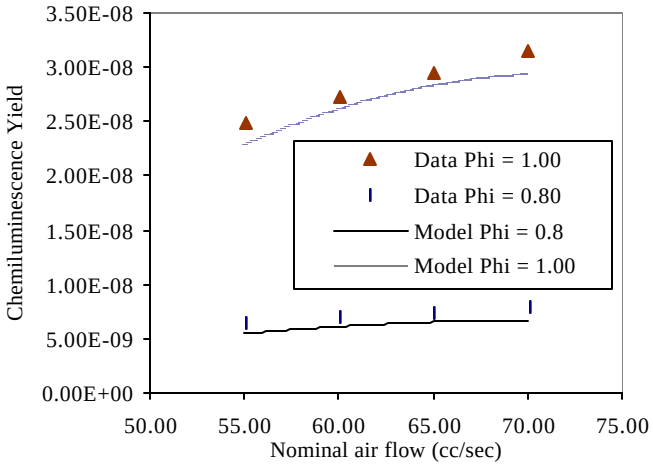

Figure 8. Comparison between modeled and experimental CH* chemiluminescence variation with nominal air flow

respectively. The variation is shown at two representative

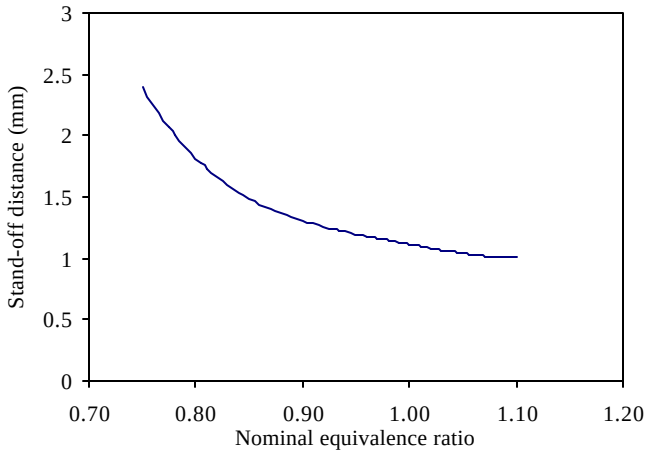

Figure 9. Flame standoff distance variation with nominal equivalence ratio

equivalence ratios (1 and 0.8). The model predicts the OH* variation with flow rate reasonably well. The CH* dependence is also captured, the discrepancy not exceeding that shown in Fig. 6 for the variation with equivalence ratio.

The excellent match between experimental data and model

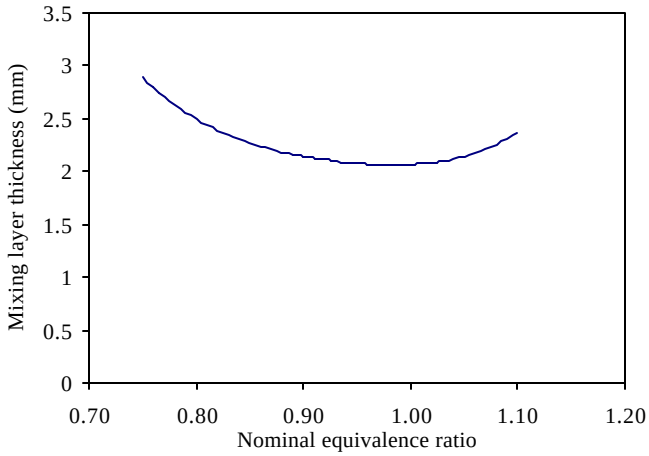

Figure 10. Mixing layer thickness variation with nominal equivalence ratio

alone cannot be considered a measure of the quality of the

model due to the large number of free parameters. The validity of the model comes from the fact that the variation of parameters with flow rate and equivalence ratio can be explained by analyzing the physics of the burning conditions for this type of experimental apparatus.

This analysis is presented in Section five. As a part of the modeling results, the parameter variations are given in figures 9 through 11. Figure 9 shows the variation of flame standoff distance with equivalence ratio. Figure 10 illustrates how the mixing layer thickness varies with nominal equivalence ratio. Figure 11 shows the difference between the lean equivalence

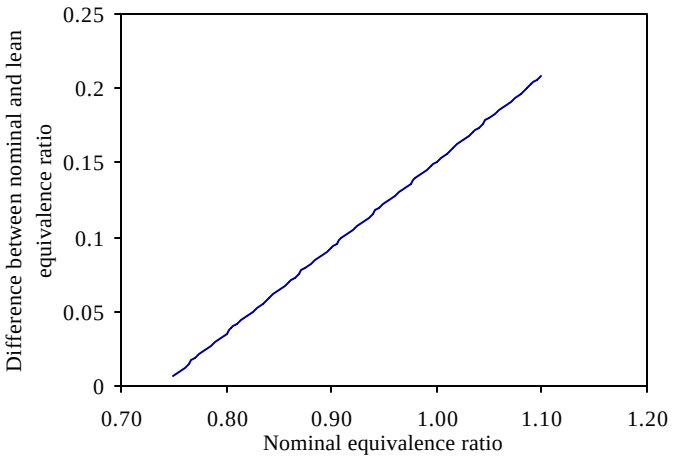

Figure 11. Variation of the difference between nominal and lean equivalence ratio with nominal equivalence ratio

ratio and the nominal equivalence ratio as a function of nominal equivalence ratio.

All parameters in the model were taken as constant over the variation of flow rates for which experimental data was obtained. The effect of flow rate on burning conditions is in general not insignificant but the range of flow rates considered in this study do not require consideration of these factors. Flame base diameter for example was considered constant at 13 mm for all conditions. Although the flame base diameter does not remain absolutely constant over the conditions considered , the assumption presents an adequate approximation for the purposes of this model.

5. DISCUSSION OF MODELING RESULTS

The parameter variations shown in Figs 9-11 were not known a priori. Some general observations about the burning conditions of the experimental setup lead to the development of equations 3 and 4. The variation of the parameters forced by matching the model to the data gives a more detailed insight into what effects are important under what conditions.

Flame standoff distance is seen to increase drastically as the nominal equivalence ratio approaches blow-off conditions near an equivalence ratio of 0.7. The flame moves away from the burner rim under leaner conditions because the burner rim is a very effective heat sink. The limit of this movement is blow-off where the fluid mechanical conditions are such that stable burning can no longer be supported.

As the flame lifts further and further from the rim, the shear layer between the main premixed gas jet and the co-flow of air is given more and more time to develop. The lifting off of the flame is the reason why the mixing layer thickness increases for lean mixtures as seen in Fig. 10.

A measure of how well the shear layer mixes the flows of premixed gas and air is given by the difference between the lean equivalence ratio at the edge of the flame and the main stream nominal equivalence ratio. Figure 11shows that the mixing with the co-flow of air at lean equivalence ratios is much less important than at higher equivalence ratios. The mixing of air with the main premixed flow is not only a function of the mixing layer thickness but also depends on the exact nature of the interaction between the air flow and the exiting premixed gas jet. The key to understanding the interaction is noticing that the flame base diameter is larger than the exit diameter of the burner rim. In other words, the premixed gas must not only travel up to reach the flame front, but also radially out.

The outward flow of the premixed gas is due in part to the shear layer immediately above the rim. The dominant cause for the outward flow however, is the pressure drop across the flame. Gases are drawn into the flame front. The higher the flame speed, the higher the pressure drop. The flame surface can be said to suck the premixed jet towards itself. For strong burning

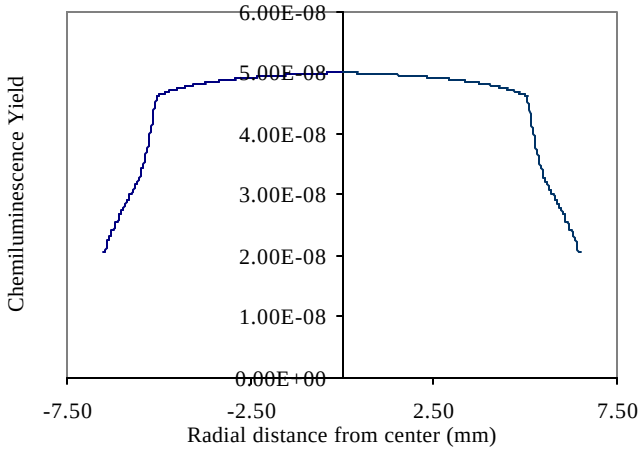

Figure 12. Radial dependence of modeled OH* chemiluminescence

mixtures, the flame sits very close to the burner rim and the velocity vector of the premixed gas burned at the base of the flame is almost perpendicular to the co-flow of air. Thus, strong burning mixtures can be expected to exhibit better mixing with air than weak burning mixtures. Figure 11 shows that the greatest difference between nominal equivalence ratio and flame edge equivalence ratio exists for the strongest burning mixture as explained in the above paragraphs.

To examine the model results further, it is helpful to compare the calculated radial variation of chemiluminescence with the experimentally obtained variation shown in Fig. 3 and Fig. 4.

Figure 12 shows the modeled OH* chemiluminescence variation over the diameter of the modeled flame. The chemiluminescence model variation is similar to that of Fig. 3. There are however some notable differences. The OH* chemiluminescence observed experimentally rises less quickly radially whereas the model predicts a steep rise, followed by another ten percent increase in approaching the flame tip region. The experimentally determined OH* chemiluminescence exhibits

a decrease in the flame tip region where the flame speed is significantly increased due to the curvature induced pre-heating. The discrepancy is clearly due to the flame model's neglect of curvature effects.

Modeled radial CH* chemiluminescence variation is not shown here for brevity. The variation is very similar to that for the modeled OH* chemiluminescence. The decrease in CH* chemiluminescence observed near the flame tip experimentally (see Fig. 4) is not obtained in the model for the same reasons described above for OH*.

The success in modeling OH* chemiluminescence on a global level allows the accurate interpretation of experimental measurements under various experimental conditions. The model ties the presence of OH* chemiluminescence strongly to the presence of HCO which is a major intermediate in all hydrocarbon oxidation. HCO has been proposed as an indicator for heat release rate by Najm et al. (1998). The study showed that HCO is a good indicator of heat release under steady and unsteady conditions and even near extinction. OH* chemiluminescence provides an indirect measure of HCO and can be measured with relative ease compared with a more complex PLIF setup.

CH* chemiluminescence is a less appropriate measure of heat release for methane combustion because the C_2-branch only accounts for several percent of the total carbon flow (Najm et al., 1998). For higher hydrocarbon fuels however, CH* may well prove to be a suitable indicator of heat release. For methane and natural gas combustion CH* the local and global measurement of CH* can provide valuable insight into the local or global burning conditions, especially when these measurements complement OH* chemiluminescence measurements.

The chemiluminescence model used to achieve the above described results is a rather crude model which omits some important characteristics of a Bunsen burner flame such as flame curvature and preheating for example. The goal here was to show that chemiluminescence need not be modeled in every detail in order for the global measurement of chemiluminescence to be more clearly understood. The chemiluminescence model provides the experimenter with a stronger sense of what factors influence the measurement and thus contribute to a more accurate interpretation of the measurement. Furthermore, the chemiluminescence model provides a starting point for determining what factors may be important when interpreting dynamic chemiluminescence measurements.

6. SUMMARY AND CONCLUSIONS

The global OH* and CH* chemiluminescence from a methane Bunsen burner flame in a co-flow of air was successfully modeled using detailed chemical kinetics and a low order heat loss model. The model parameter variations obtained in matching the model to the experimental data were able to be explained fully by analyzing the general burning process of the flame under various experimental conditions.

The radial variation of OH* and CH* were not modeled accurately due to the model's neglect of curvature effects.

The study provides an important link between OH* chemiluminescence and HCO which is a major hydrocarbon oxidation intermediate previously shown to be a good indicator of heat release (Najm et al., 1998). Although CH* chemiluminescence is not an adequate indicator of heat release for methane combustion, the measurement of CH* chemiluminescence can provide important insights into local and global burning conditions.

The chemiluminescence model presented above covers a broad range of equivalence ratios and helps solidify the production paths of OH* and CH* chemiluminescence.

The burning condition model used in the study is a very low order estimate of the true experimental conditions and still yields an accurate model for global chemiluminescence. The methodology outlined in the present paper can thus be applied to more complicated flame environments without requiring a prohibitive amount of modeling.

ACKNOWLEDGMENTS

The authors would like to acknowledge the support of Mr. Ludwig Haber by a NSF Graduate Fellowship.

REFERENCES

Devriendt, K., and Peeters, J., 1997, "Direct identification of the $C_2H(X^2\Sigma^+) + O(^3P) \rightarrow CH(A^2\Delta) + CO$ reaction as the source of the $CH(A^2\Delta \rightarrow X^2\Pi)$ chemiluminescence in C_2H_2/O/H atomic flames", *Journal of Physical Chemistry*, Vol. 101, pp. 2546-2551

Dandy, D. S., and Vosen, S. R., 1992, "Numerical and experimental studies of hydroxyl radical chemiluminescence in methane-air flames", *Combustion Science and Technology*, Vol. 82, pp. 131-150

Egolfopoulos, F. N., 1994, "Geometric and radiation effects on steady and unsteady strained laminar flames", *25th Combustion Symposium (international*), pp. 1375-1381

Ferguson, R. E., and Broida, H. P., 1954, "Atomic flames: Spectra, 'Temperatures', and products", *5th Combustion Symposium (international)*, pp. 754-765

Haber, L.C., and Vandsburger, U., 2000, "OH* chemiluminescence modeling advances", to be submitted to *Combustion Science and Technology*

Garland, N. L., and Crosley, D. R., 1986, "On the collisional quenching of electronically excited OH, NH and CH in flames", *21st Combustion Symposium (international)*, pp.1693-1702

Kee, R. J., Grcar, J. F., Smooke, M. D., and Miller, J. A., 1993, "A fortran program for modeling of steady laminar one-dimensional premixed flames", *SANDIA* report SAND85-8240

Langhorne, P. J., 1988, "Reheat buzz: An acoustically coupled combustion instability. Part 1. Experiment", *Journal of Fluid Mechanics*, Vol. 193, pp. 417-443

Najm, H. N., Paul, P. H., Mueller, C. J., and Wyckoff, P. S., 1998, "On the adequacy of certain experimental observables as measurements of flame burning rate", *Combustion and Flame*, Vol. 113, pp. 312-322

Porter, R. P., Clark, A. H., Kaskan, W. E., and Browne, W. E., 1966, "A study of hydrocarbon flames", *11th Combustion Symposium (international)*, pp. 907-917

Samaniego, J.-M., Egolfopoulos, F. N., and Bowman, C. T., 1995, "CO_2* chemiluminescence in premixed flames", *Combustion Science and Technology*, Vol. 109, pp. 183-203

Samaniego, J. M., Yip, B., Poinsot, T., and Candel, S., 1993, "Low frequency combustion instability mechanisms in a side dump combustor", *Combustion and Flame*, Vol. 94, pp. 363-380

Smith, P.G., Golden, D. M., Frenklach, M., Moriarty, N. W., Eiteneer, B., Goldenberg, M., Bowman, C. T., Hanson, R., Song, S., Gardiner, W. C. Jr., Lissianski, V., and Qin, Z., 1999 `http://www.me.berkeley.edu/gri_mech/`

Sun, C. J., Sung, C. J., Law, C. K., 1994, "On adiabatic stabilization and geometry of Bunsen flames", *25th Combustion Symposium (international)*, pp. 1391-1398